AIAA 81-1021R

Shock-Capturing Algorithm for the Navier-Stokes Equations

R. P. Reklis* and P. D. Thomas†
Lockheed Palo Alto Research Laboratory, Palo Alto, Calif.

An implicit numerical algorithm for the unsteady Euler and Navier-Stokes equations is presented. This algorithm is based on flux vector splitting to retain the proper direction of information flow in the algorithm's numerical domain of dependence and on a finite volume formulation to ensure conservation. Results from a one-dimensional shock-tube problem show that expansions are accurately computed and shocks are sharply defined. The algorithm remains stable and accurate for shocks of seemingly unlimited strength and yields an improvement in convergence rate. The use of these methods for higher-dimensional viscous flows is discussed, and results from a two-dimensional flat-plate boundary-layer problem show good accuracy on a nonuniform grid.

Introduction

FLUX-vector-splitting ideas introduced recently by Steger and Warming[1] seem to indicate possibilities for improving methods for the Euler and Navier-Stokes equations. Initial studies indicate that advantages may be obtained but that problems with accuracy may arise. Considerable fundamental groundwork is necessary to fully understand the properties of flux-vector-splitting schemes and to obtain their advantages for practical problems. Some of this groundwork is presented here.

The flux-vector-splitting idea, as used in this work, is associated with a local linearization of the time-dependent Euler equations in conservation form. A Jacobian matrix arises from linearization of the flux terms in these equations. This has three eigenvalues associated with the three velocities at which disturbances propagate in an ideal inviscid fluid. The flux vectors may be split into three corresponding parts. Once the Euler equations are written in terms of split fluxes, each flux piece may be treated with separate spatial differencing, so that the domain of dependence of the spatial differencing retains the direction of disturbance propagation associated with each flux piece. If the fluxes are not split, unconditionally stable implicit schemes may be obtained only by addition of an artificial smoothing term. Flux-splitting methods may be devised that require no artificial smoothing terms and have improved convergence rates in cases treated thus far.

For purely inviscid flows, Moretti[2] presented a scheme for a nonconservative form of the flow equations that properly accounts for the domain of dependence by an artful splitting of the spatial derivative terms into subgroups that can be identified with the characteristic directions. The derivative operators in each subgroup are approximated separately by either forward or backward difference operators as dictated by the signs of the characteristics. An equivalent scheme for the nonconservative form of the inviscid equations was presented by Chakravarthy,[3] who used the concepts of matrix algebra to develop the scheme in a more formal and deterministic fashion than did Moretti.[2] These schemes have proved much more stable and accurate than previous schemes that ignored the implications of characteristics theory. The new schemes, however, cannot be applied to the conservative form of the equations and have not been attempted for viscous flows. Steger and Warming[1] presented a stable implicit algorithm for the conservative form of the inviscid flow equations. This algorithm splits the terms representing fluxes of mass, momentum, and energy into two subterms associated with positive and negative eigenvalues of the flux vector Jacobian matrices. In the present work a closely related approach is taken; however, all three flux pieces are retained and a finite-volume formulation is used.

In a finite volume formulation, spatial discretization of a system of conservation laws is arrived at by an integration of the conservation laws over small cells. The resulting discretized equations involve differences between fluxes of the conserved quantities at the cell boundaries. Use of this type of formulation ensures that the resulting algorithm will maintain conservation, since fluxes are computed uniquely at cell boundaries and the flux out of one cell is necessarily the flux into its neighbor.

In the present work flux vector splitting is coupled with a finite volume formulation to obtain an algorithm that is implicit and unconditionally stable, time-accurate to first order, spatially accurate to second order, and suitable for use on arbitrary grids. Results from the use of this algorithm are given for two model problems that have been chosen to embody features found in more general flows. These model problems include solution of the Euler equations for a one-dimensional shock-tube problem and of the Navier-Stokes equations for a flat-plate boundary layer. The one-dimensional shock-tube problem demonstrates the performance of the algorithm for an expansion wave, a contact discontinuity, and a shock discontinuity. The boundary-layer problem demonstrates a solution on a nonuniform grid and brings forth some of the problems that arise from addition of viscous terms.

Flux Splitting

Mathematical demonstrations in this and following sections will be made in one dimension as far as possible for simplicity. Viscous terms are treated by standard central-difference methods and are not further discussed.

Flux vector splitting comes from a local linearization of the Euler equations. These may be written in conservation form as follows:

$$q_t + f_x = 0 \tag{1}$$

where

$$q = \begin{bmatrix} \rho \\ \rho v \\ \rho v^2/2 + p/[\gamma(\gamma-1)] \end{bmatrix} \qquad f = \begin{bmatrix} \rho v \\ \rho v^2 + p/\gamma \\ \rho v^3/2 + pv/(\gamma-1) \end{bmatrix}$$

Presented as Paper 81-1021 at the AIAA Fifth Computational Fluid Dynamics Conference, Palo Alto, Calif., June 22-23, 1981; submitted July 6, 1981; revision received Jan. 22, 1982.

*Research Scientist. Member AIAA.
†Staff Scientist. Member AIAA.

and where γ is the ratio of specific heats. The vector q is a vector of mass, momentum, and energy densities, and the vector f is a vector of mass, momentum, and energy fluxes. The pressure p and density ρ are normalized by pressure and density at reference conditions, and the fluid velocity v is normalized by a reference sound speed. In this normalization the equation of state for a perfect gas becomes

$$p/\rho = T = c^2$$

where c is local sound speed and T is temperature.

Equation (1) is locally linearized[5] by employing the Jacobian matrix F where

$$F = \partial f/\partial q \qquad \mathrm{d}f = F\mathrm{d}q$$

and by employing the homogeneous property of the Euler equations

$$f = Fq$$

The Jacobian matrix may be diagonalized by a similarity transformation using a known[5] matrix M,

$$MFM^{-1} = \begin{bmatrix} v & & \\ & v+c & \\ & & v-c \end{bmatrix}$$

A spectral decomposition[6] of F may be accomplished with the projection operators

$$P_1 = M^{-1}\begin{bmatrix} 1 & & \\ & 0 & \\ & & 0 \end{bmatrix}M \qquad P_2 = M^{-1}\begin{bmatrix} 0 & & \\ & 1 & \\ & & 0 \end{bmatrix}M$$

$$P_3 = M^{-1}\begin{bmatrix} 0 & & \\ & 0 & \\ & & 1 \end{bmatrix}M$$

to yield

$$F = vP_1 + (v+c)P_2 + (v-c)P_3$$

The flux term may be split correspondingly,

$$f = f_1 + f_2 + f_3$$

where

$$f_1 = vP_1q \qquad f_2 = (v+c)P_2q \qquad f_3 = (v-c)P_3q$$

For the one-dimensional case these split fluxes can be written in terms of the flow variables as

$$f_1 = [v(\gamma-1)/\gamma]\begin{bmatrix} \rho \\ \rho v \\ \rho v^2/2 \end{bmatrix}$$

$$f_{\frac{2}{3}} = [(v\pm c)/2\gamma]\begin{bmatrix} \rho \\ \rho(v\pm c) \\ \rho v^2/2 + p/(\gamma-1) \pm \rho vc \end{bmatrix}$$

The flux pieces obtained from the spectral decomposition described above are related to fluxes of entropy and Riemann invariants that are associated with the characteristics of the Euler system. It is important to note that each flux piece is associated with a speed and direction for disturbance propagation in the fluid, that is, with an eigenvalue of F.

This flux splitting can readily be generalized to higher dimensions and may be applied on arbitrarily moving grids. A higher-dimensional Euler system retains its conservation form when subjected to an arbitrary coordinate transformation. Such a transformation in three dimensions may be expressed as

$$\xi = \xi(x,y,z,t)$$
$$\eta = \eta(x,y,z,t) \qquad J = \frac{\partial(x,y,z)}{\partial(\xi,\eta,\zeta)}$$
$$\zeta = \zeta(x,y,z,t)$$
$$\tau = \tau(t)$$

where ξ,η,ζ form the transformed coordinates. When this transformation is applied, fluxes are associated with the new variables ξ,η,ζ and may be split as described above. For the ξ direction,

$$e_1 = J\nabla\xi\cdot v + J\xi_t \qquad e_{\frac{2}{3}} = J\nabla\xi\cdot v + J\xi_t \pm c\,|J\nabla\xi|$$

are the eigenvalues. The eigenvalue e_1 is triply degenerate and

$$f_1 = [e_1(\gamma-1)/\gamma]\begin{bmatrix} \rho \\ \rho u \\ \rho v \\ \rho w \\ \rho v^2/2 \end{bmatrix} \tag{2}$$

$$f_{\frac{2}{3}} = [e_{\frac{2}{3}}/2\gamma]\begin{bmatrix} \rho \\ \rho(u \pm cJ\xi_x/|J\nabla\xi|) \\ \rho(v \pm cJ\xi_y/|J\nabla\xi|) \\ \rho(w \pm cJ\xi_z/|J\nabla\xi|) \\ \rho v^2/2 + p/(\gamma-1) \pm \rho cJ\nabla\xi\cdot v/|J\nabla\xi| \end{bmatrix}$$

where u, v, and w are the components of fluid velocity v. Within the context of a finite volume formulation, the metric vector $J\nabla\xi$ is a vector normal to a cell face and its magnitude is equal to the face area. The inverse transformation Jacobian J is equal to the cell volume.

Finite-Volume Spatial Discretization

To form the difference equations, a gridwork of nodes is laid out on which the computation will be performed. Flowfield variables are computed only at these nodes. In a finite volume formulation, the nodes form the centers of cells that cover the grid. Discretized formulas are arrived at by spatial integration of the governing equations written in conservation form. In one dimension on a uniform grid, for example, cell walls lie midway between the nodes, as illustrated in Fig. 1. Spatial integration of the Euler equation (1) across the cell whose center is at $x=a$, given by

$$\int_{a-\Delta x/2}^{a+\Delta x/2} (q_t + f_x)\,\mathrm{d}x = 0$$

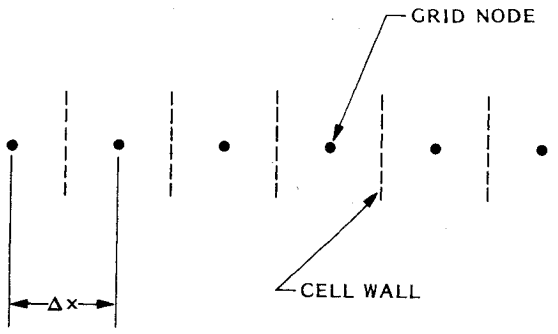

Fig. 1 One-dimensional finite volume grid showing cell boundaries.

results in

$$\Delta x q_t(a) + f(a+\Delta x/2) - f(a-\Delta x/2) + 0(\Delta x^3) = 0$$

Ignoring the $q_t(a)$ time derivative term for the time being, a description will now be given of a means by which the flux terms can be evaluated using the flux-vector-splitting ideas presented above. As information from which to form the flux vectors is available only at the grid nodes, it must be carried to the cell walls by either interpolation or extrapolation. The use of two-point linear interpolation,

$$f(a+\Delta x/2) = [f(a+\Delta x) + f(a)]/2$$

results in a method equivalent to a centrally differenced finite difference method.[3] Instead, the flux vectors are split,

$$f(a+\Delta x/2) = f_1(a+\Delta x/2) + f_2(a+\Delta x/2) + f_3(a+\Delta x/2)$$

where each piece is treated separately. The densities of mass, momentum, and energy q are extrapolated using two-point forward or backward formulas, depending on the sign of the eigenvalue associated with each flux piece. These extrapolated values are used to form the flux pieces. If, for example, the eigenvalues associated with f_1 were positive, the q^* vector would be formed,

$$q^* = [3q(a) - q(a-\Delta x)]/2$$

and the flux piece f would be formed from the flow variables q^*. In the case of higher dimensions, transformations are used to map the physical grid onto a uniform computational grid lying along Cartesian axes. Computational cell boundaries lie halfway between the nodes, and flow variables are extrapolated as above to form the flux pieces at the cell faces. As can be seen from Eq. (2), the flux pieces are functions of geometric quantities, such as $J\nabla\xi$. This geometric information is not directional and is always interpolated. If geometric information is extrapolated, significant errors result when nonuniform physical grids are used.

The choice of direction for extrapolation as described above depends on the sign of the eigenvalue associated with each flux piece. These eigenvalues are available only at grid nodes, and an ambiguous choice results if they change sign from one cell to the next. This occurs at sonic points, shocks, contact discontinuities, etc. Under such conditions flowfield information is interpolated to form the flux piece. It is emphasized that this finite volume formulation remains conservative no matter how the fluxes are computed at cell faces.

Implicit Time Differencing

The spatial discretization discussed in the last section can be combined with either explicit or implicit time differencing. We have chosen to use implicit time differencing in order to produce a scheme that will be stable for large time steps. Application of implicit time differencing, in the delta form,[5] to the Euler equations in one dimension with split flux vectors yields

$$\left\{\Delta x I + \frac{\Delta t}{R}\left\{\frac{\partial}{\partial q}\left[f_1\left(a+\frac{\Delta x}{2}\right) + f_2\left(a+\frac{\Delta x}{2}\right) + f_3\left(a+\frac{\Delta x}{2}\right)\right]\right.\right.$$
$$\left.\left. - \frac{\partial}{\partial q}\left[f_1\left(a-\frac{\Delta x}{2}\right) + f_2\left(a-\frac{\Delta x}{2}\right) + f_3\left(a-\frac{\Delta x}{2}\right)\right]\right\}\right\}\Delta q$$
$$= -\Delta t\left\{\left[f_1\left(a+\frac{\Delta x}{2}\right) + f_2\left(a+\frac{\Delta x}{2}\right) + f_3\left(a+\frac{\Delta x}{2}\right)\right]\right.$$
$$\left. - \left[f_1\left(a-\frac{\Delta x}{2}\right) + f_2\left(a-\frac{\Delta x}{2}\right) + f_3\left(a-\frac{\Delta x}{2}\right)\right]\right\} \tag{3}$$

where Δq is the difference in q between new and old time steps, Δt is the time step, and R is a constant used to improve the damping of high-frequency waves. The constant R affects neither the first-order time accuracy nor the second-order spatial accuracy of the scheme and will be discussed further below. Jacobian matrices of the form

$$\frac{\partial}{\partial q} f_1(a+\Delta x/2) \tag{4}$$

appear on the left-hand side of Eq. (3). As these are evaluated at cell boundaries, information must be extrapolated from the grid nodes to form them. Information to form these matrices is obtained as described in the last section, except that, instead of using two-point formulas, information is used from only one point. Two-point formulas are used on the right-hand side of Eq. (3) so as to maintain second-order spatial accuracy in the solution. By the use of information from only one point in forming the left-hand side, the Jacobian matrix (4) becomes an operator on the vector $\Delta q(a)$ or $\Delta q(a+\Delta x)$ and the left-hand side remains a block tridiagonal operator on the vector Δq. This has been done chiefly to allow continued use of an existing subroutine for solving block tridiagonal systems.

Stability and Time Accuracy

As a stability analysis for the nonlinear system given in Eq. (3) is difficult to perform, a similar scheme is applied to the linear model equation

$$\phi_t + c\phi_x = 0$$

to gain insight into the stability of the nonlinear system. If a scheme similar to that given in Eq. (3) is applied to the trial solution $e^{i\omega\Delta x}$, one finds, after one time step, $ge^{i\omega\Delta x}$ where

$$g = 1 - \frac{\alpha(3/2 - 2e^{-i\omega\Delta x} + \tfrac{1}{2}e^{-2i\omega\Delta x})}{1 + (\alpha/R)(1 - e^{-i\omega\Delta x})} \tag{5}$$

where $\alpha = c\Delta t/\Delta x$ is the Courant number. The scheme is unconditionally stable for this model problem. The magnitude of g as a function of $\omega\Delta x$ for several Courant numbers with $R = \frac{1}{2}$ is shown in Fig. 2 together with the magnitude of the stability factor g for a scheme using central differencing as a comparison. As can be seen, the central scheme does not damp two-mesh waves ($\omega\Delta x = \pi$). For this reason, an additional smoothing term must be added to such a scheme. For two-mesh waves, Eq. (5) becomes

$$g = 1 - 4\alpha/(1 + 2\alpha/R)$$

and the reason for the factor R can be seen. The choice $R = \frac{1}{2}$ will force $g = 0$ in the limit $\alpha \to \infty$.

Because the solution of the model equation must be in the form $\phi(x-ct)$, the factor g must approximate $e^{-i\omega c\Delta t}$ if the

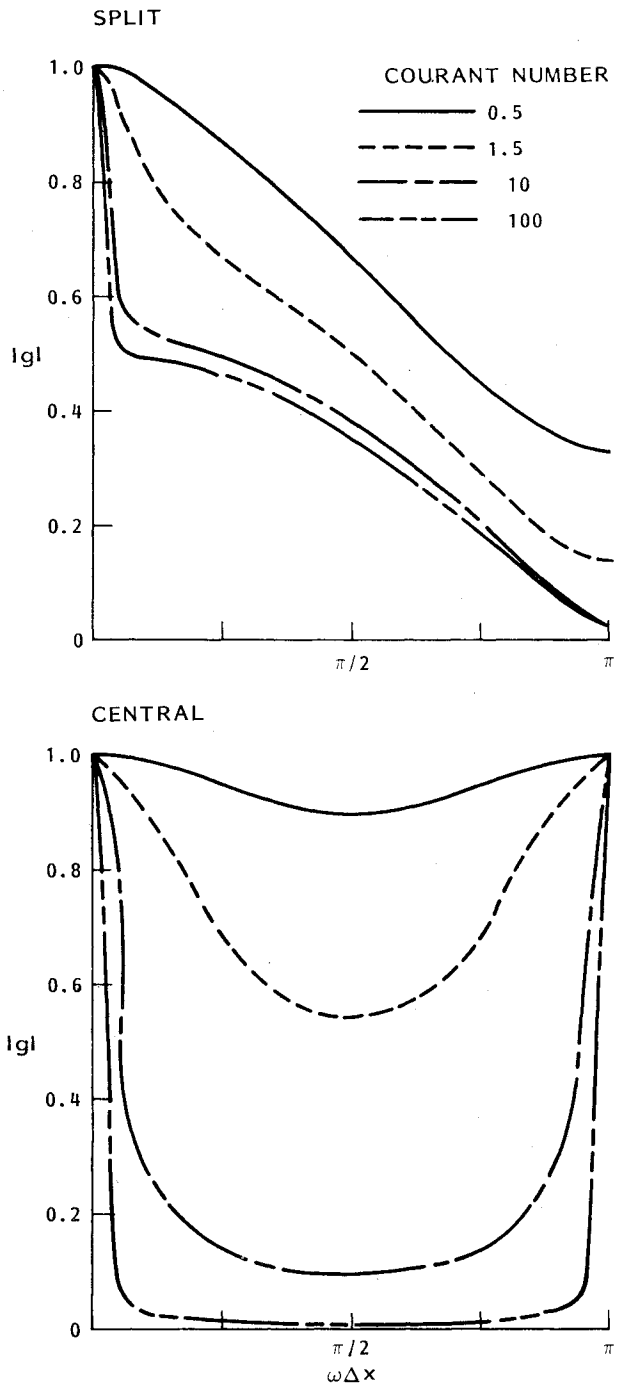

Fig. 2 Damping factors for the split and central schemes.

scheme is to be time-accurate. Note that

$$g = 1 - (c\Delta t/\Delta x)\,[i\omega\Delta x + 0(\Delta x^3)\,]\,[1 + 0(c\Delta t/R\Delta x)\,]$$

$$= e^{-i\omega c\Delta t} + 0(c\Delta t/\Delta x)^2$$

and that the scheme is thus first-order accurate in time for any value of R.

The above analysis is equally valid for a linear system,

$$\phi_t + F\phi_x = 0$$

where F is a matrix with real eigenvalues. A spectral decomposition similar to that used in the flux-splitting procedure given above would separate this linear system into uncoupled equations similar to the linear model equation discussed above. The Euler system is nonlinear, and the Jacobian matrices

$$F = \frac{\partial f}{\partial q}$$

are functions of q. Further, the homogeneity property does not hold for the flux pieces. That is,

$$F_l = \frac{\partial f_l}{\partial q} = \frac{\partial}{\partial q} e_l P_l q \neq e_l P_l$$

It is important to use the Jacobian matrices F not the projection operators as left-hand-side operators. Use of the projection operators results in a conditionally stable scheme.[1]

The claim is often made that some implicit scheme for the Euler equations is unconditionally stable. Combinations of time step, boundary, and initial conditions can be put together, nonetheless, for which the scheme will diverge. Such a claim implies that the scheme shows no stability bound on Courant number when applied to a linear model equation and that there exists some class of initial and boundary conditions for which it is stable for the Euler equations. In that sense the split-flux scheme described above is unconditionally stable. The flux-splitting approach widens the range of conditions under which stability is obtained for the two model problems discussed below.

One-Dimensional Shock Tube

A shock tube is formed by separating gas in a tube into two sections by a diaphragm. The gas on each side may differ in composition, pressure, temperature, etc. When the diaphragm is ruptured, a shock, an expansion, and a contact surface discontinuity move away from the position of the diaphragm at characteristic velocities. In the ideal case considered here the diaphragm is in the center of a tube lying along the x axis and extending to infinity in both directions. It is filled with an ideal gas whose ratio of specific heats is 1.4 and which is initially at a constant temperature. The pressures on each side of the diaphragm, however, differ by a factor of 5. The exact solution of the Euler equations for such a problem may be written in terms of a single variable x/t, and it is the constant velocities of the various features which are of significance. For this reason the problem is solved on an expanding grid and grid velocity is accounted for through the arbitrary mapping procedure discussed above. The grid expands linearly with time to produce a moving coordinate system in which the problem has a steady-state solution as $t \to \infty$. All grid points are given a velocity from $-c$ to $2c$, where c is the initial sound speed, and are assigned initial positions on a uniform grid at time $t = 1$. The initial conditions are spatially uniform on either side of the diaphragm, which bursts at time $t = 1$.

The plot of density as a function of x/t presented in Fig. 3 shows the final converged locations of the expansion, contact discontinuity, and shock found by the algorithm using flux splitting (split algorithm). A similar plot is shown in Fig. 4 for densities computed by an algorithm in which interpolation of the fluxes is used to obtain fluxes at cell walls (central algorithm). This algorithm requires smoothing for stability, and care must be taken not to oversmooth the features. A fourth-order smoothing term is used which allows formation of a steady converged solution if the Courant number $\Delta t/\Delta x$ (based on the reference sound speed $c = 1$) is held fixed. The two solutions are comparable and accurately predict the expansion, contact discontinuity, and shock. The exact solution is given by the solid line. Although seemingly trivial, the small undershoot at the foot of the shock produced by the central algorithm is of significance and does not appear in the split solution.

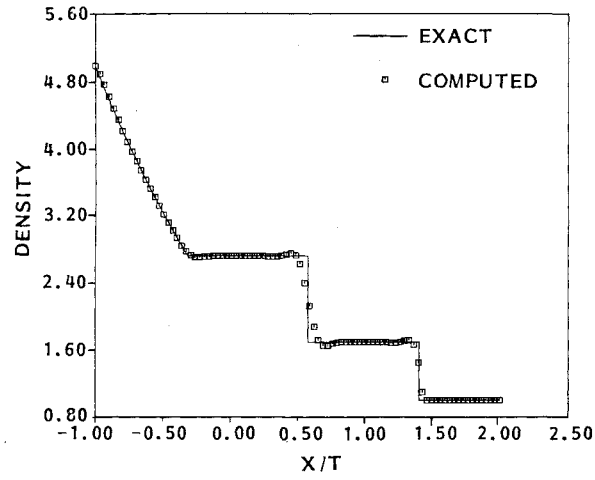

Fig. 3 Density distribution in an ideal shock tube as computed by the split scheme.

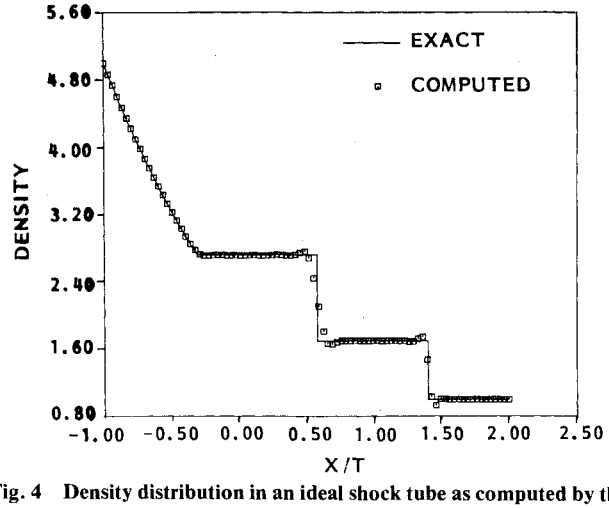

Fig. 4 Density distribution in an ideal shock tube as computed by the central scheme.

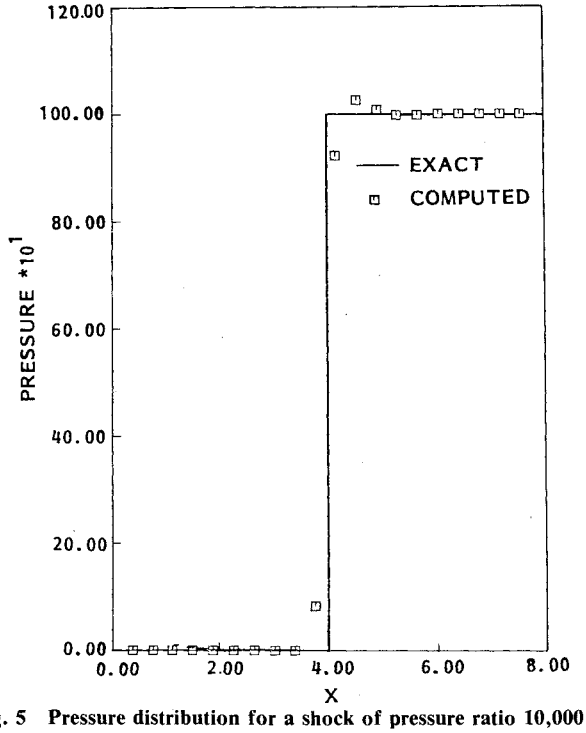

Fig. 5 Pressure distribution for a shock of pressure ratio 10,000 as computed by the split scheme.

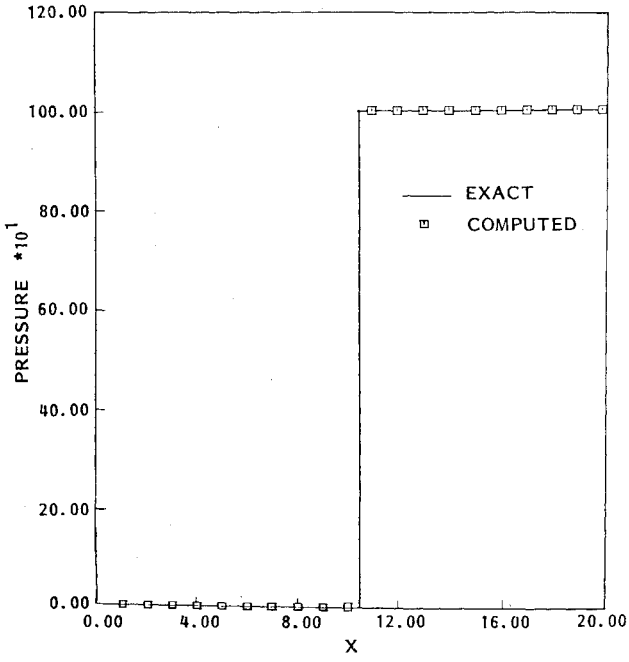

Fig. 6 Pressure distribution for a shock of pressure ratio 1000 as computed by the split scheme with shock sharpening.

For shocks with pressure ratios greater than about 10, the preshock undershoot of the central scheme produces a negative density and the calculation fails disastrously. As evidence that the split scheme does not suffer from this problem, a shock of pressure ratio 10,000 is shown in Fig. 5 as captured by the split scheme. The solution retains the same character as for a weak shock. There appears to be no limit on the strength of the shock that the split scheme will capture successfully.

The sharpness of the shock, as captured by the split scheme, may be improved for a steady shock, in one dimension, by an alteration of the manner in which information is extrapolated at cell faces between grid points, where the eigenvalues change sign. Doing this produces the result shown in Fig. 6 for a shock with pressure ratio 1000.

The shock-tube problem, as well as providing a test of accuracy, also serves to demonstrate the convergence rate of the split scheme for a problem that possesses a time-asymptotic steady-state solution. For Courant numbers less than unity, both split and central schemes are time-accurate and the rate of convergence improves as the Courant number is increased. At Courant numbers greater than 1, time accuracy is not guaranteed and the convergence rate may or may not continue to improve as the Courant number is increased. Because of the care with which numerical domains of dependence have been treated in the split scheme, disturbances must at least travel in the right direction. Convergence histories for Courant numbers 1, 10, 100, and 1000 are shown for the split scheme in Fig. 7, which shows that the convergence rate continues to improve for large Courant numbers. The only limit is that the computer produces a floating point overflow when the time step reaches 10^{40}.

The split scheme is unconditionally stable for this problem. This is not the case for the central algorithm, for which convergence histories are shown in Fig. 8 for Courant numbers 1, 5, and 10. The convergence rates are essentially the same for the two schemes for a Courant number of 1, where both are still time-accurate. The convergence rate continues to improve for the central scheme up to a Courant number of 10. The central scheme becomes unstable for larger Courant numbers.

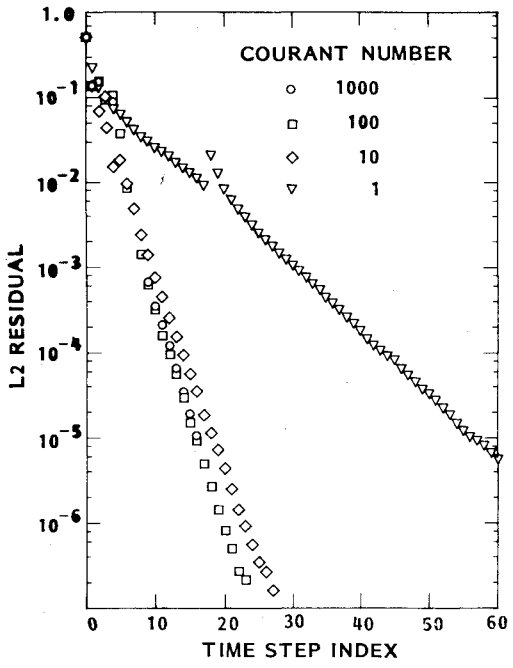

Fig. 7 Convergence history for the split scheme as a function of the number of time iteration steps.

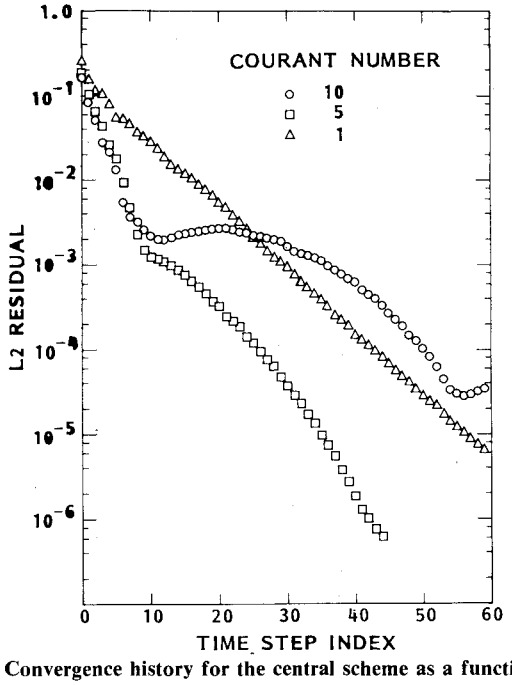

Fig. 8 Convergence history for the central scheme as a function of the number of time iteration steps.

Flat-Plate Boundary Layer

The Blasius solution[7] for incompressible flow over a semi-infinite flat plate at zero incidence is well known. The solution is self-similar in terms of the variable $y\sqrt{u_\infty/\nu x}$ where y is distance normal to the plate, u is freestream velocity, and ν is kinematic viscosity of the fluid. The boundary layer thickens as $\sqrt{x}$.

This flat-plate boundary-layer problem is solved in a parabolic coordinate system on the two-dimensional grid shown in Fig. 9. The thin-layer approximation for the viscous terms is used; only viscous terms that involve derivatives in the plate normal direction are kept. The boundary condition at the leading edge of the plate is taken from the Blasius solution. A half-cell outflow boundary condition similar to that discussed by Thomas and Lombard[4] is used. The velocity

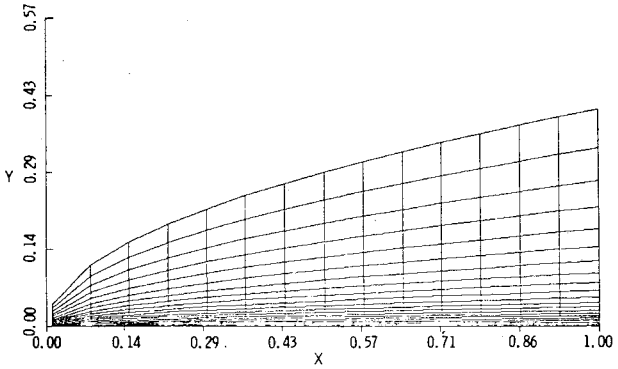

Fig. 9 Grid for the flat-plate boundary-layer problem.

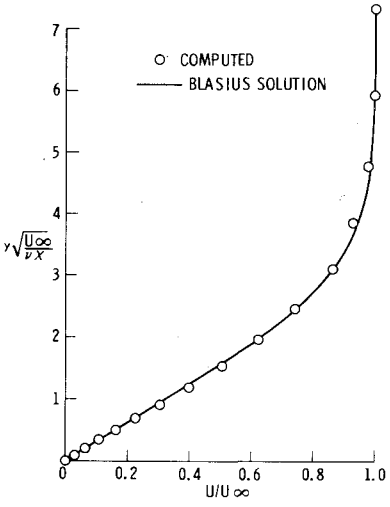

Fig. 10 Boundary-layer velocity profile as computed by the hybrid scheme.

at the surface is fixed at zero, as is the derivative of the pressure normal to the surface. Initial conditions are taken from the Blasius solution.

Two problems with solution accuracy were encountered in the first attempt to solve this problem with the split scheme. In that attempt the flux pieces were extrapolated from the grid nodes to the cell faces. These flux pieces contain geometric information as well as flowfield information. When applied to the grid shown in Fig. 9, with boundary and initial conditions suitable for uniform inviscid flow, the scheme produced 10% pressure fluctuations in its solution. This problem has been corrected by interpolating geometric quantities properly, as described earlier.

A second accuracy problem is caused by the dissipative terms that are generated naturally by the split scheme. Even though no artificial smoothing term is added, effective dissipative terms appear which have the same form. These become important in the boundary-layer calculation. It is simpler to analyze this effect by considering the scheme applied to a uniform grid ($\Delta x, \Delta y$ constant). Under these circumstances, there is an effective smoothing term in the streamwise momentum equation, of the form

$$\Delta x c \Delta t \delta_{yyyy} \rho u \tag{6}$$

where δ_{yyyy} is a central fourth-difference operator. The artificial explicit smoothing term that normally is added to the central scheme is of the same form,

$$s \Delta x \Delta y \delta_{yyyy} \rho u$$

where s is a constant ($s < 1/8$). For this boundary-layer calculation, $c\Delta t \gg \Delta y$ and consequently the natural dissipation of the split scheme is orders of magnitude larger than the artificial smoothing added to the central scheme. It is unfortunately not possible to adjust the natural smoothing with a controllable parameter, such as s.

The question remains: Is the natural smoothing too large? This may be answered by comparing the natural smoothing to the viscous term, which has the form

$$\Delta x c \Delta t \delta_{yy} \rho u / (c\Delta y/\nu)$$

The coefficient of δ_{yy} differs from the coefficient of δ_{yyyy} in Eq. (6) by the factor $c\Delta y/\nu$, the cell Reynolds number. This may be evaluated from

$$c\Delta y/\nu \approx 5\sqrt{Re/M_\infty}/N$$

where Re is the true Reynolds number based on the distance x from the leading edge, M_∞ is the freestream Mach number, and N is the number of points in the boundary layer. This number may be quite large. Consequently the natural smoothing may dominate the viscous term, thus creating an inaccurate solution.

A straightforward way to avoid this problem is to use a hybrid scheme in which the split algorithm is applied in the streamwise direction and the central algorithm is applied in the direction normal to the plate. The velocity profile computed by the hybrid scheme is shown in Fig. 10. This flow has a freestream Mach number of 0.1 and a Reynolds number of 100,000 based on plate length. The computed profile agrees closely with the Blasius solution.

The hybrid scheme has the advantages of both methods. The solution for the boundary layer is accurate, and the scheme remains stable for streamwise Courant numbers greater than 1000. The pure central algorithm has comparable accuracy within its domain of stability, but is unstable for Courant numbers of 10 or more.

Summary

A description has been given of an implicit algorithm that uses flux-vector-splitting techniques in combination with a finite volume formulation. The stability and accuracy properties of the algorithm have been investigated for both inviscid and viscous flows. The algorithm has been applied successfully to simple flow problems involving the solution of the Euler and Navier-Stokes equations. The algorithm is accurate and has substantially greater stability than a centrally differenced algorithm. The improved stability yields increased rates of convergence in problems where a steady-state solution is sought by time relaxation. The model problems embody many features encountered in more general flows, and the present results suggest that an algorithm based on these techniques offers potential for application to problems of more practical significance.

References

[1] Steger, J. L. and Warming, R. F., "Flux Vector Splitting of the Inviscid Gasdynamic Equations with Application to Finite Difference Methods," NASA TM 78605, 1979.

[2] Moretti, G., "The λ-Scheme," *Computers and Fluids,* Vol. 7, Sept. 1979, pp. 191-205.

[3] Chakravarthy, S. R., "The Split-Coefficient Matrix Method for Hyperbolic Systems of Gas Dynamic Equations," AIAA Paper 80-0268, 1980.

[4] Thomas, P. D. and Lombard, C. K., "The Geometric Conservation Law—A Link Between Finite-Difference and Finite Volume Methods of Flow Computation on Moving Grids," AIAA Paper 78-1208, 1978; also *AIAA Journal,* Vol. 17, Oct. 1979, pp. 1030-1037.

[5] Warming, R. F. and Beam, R. M., "On the Construction and Application of Implicit Factored Schemes for Computational Laws," *SIAM-AMS Proceedings of the Symposium on Computational Fluid Dynamics,* Vol. 11, New York, 1978, pp. 85, 129.

[6] Nering, E. D., *Linear Algebra and Matrix Theory,* Wiley, London, 1963, pp. 217-225.

[7] Schlichting, H., *Boundary Layer Theory,* 1st English ed., Pergamon, New York, 1955, p. 107.